Serine hydroxymethyltransferase 2 expression promotes tumorigenesis in rhabdomyosarcoma with 12q13-q14 amplification

Thanh H. Nguyen,[1] Prasantha L. Vemu,[1] Gregory E. Hoy,[1] Salah Boudjadi,[1] Bishwanath Chatterjee,[1] Jack F. Shern,[2] Javed Khan,[3] Wenyue Sun,[1] and Frederic G. Barr[1]

[1]Laboratory of Pathology, [2]Pediatric Oncology Branch, and [3]Genetics Branch, Center for Cancer Research, National Cancer Institute, Bethesda, Maryland, USA.

The 12q13-q14 chromosomal region is recurrently amplified in 25% of fusion-positive (FP) rhabdomyosarcoma (RMS) cases and is associated with a poor prognosis. To identify amplified oncogenes in FP RMS, we compared the size, gene composition, and expression of 12q13-q14 amplicons in FP RMS with those of other cancer categories (glioblastoma multiforme, lung adenocarcinoma, and liposarcoma) in which 12q13-q14 amplification frequently occurs. We uncovered a 0.2 Mb region that is commonly amplified across these cancers and includes CDK4 and 6 other genes that are overexpressed in amplicon-positive samples. Additionally, we identified a 0.5 Mb segment that is only recurrently amplified in FP RMS and includes 4 genes that are overexpressed in amplicon-positive RMS. Among these genes, only serine hydroxymethyltransferase 2 (SHMT2) was overexpressed at the protein level in an amplicon-positive RMS cell line. SHMT2 knockdown in amplicon-positive RMS cells suppressed growth, transformation, and tumorigenesis, whereas overexpression in amplicon-negative RMS cells promoted these phenotypes. High SHMT2 expression reduced sensitivity of FP RMS cells to SHIN1, a direct SHMT2 inhibitor, but sensitized cells to pemetrexed, an inhibitor of the folate cycle. In conclusion, our study demonstrates that SHMT2 contributes to tumorigenesis in FP RMS and that SHMT2 amplification predicts differential response to drugs targeting this metabolic pathway.

Introduction

DNA amplification is one of the most frequent molecular alterations observed in human cancer (1–4). In genomic amplification events, focal chromosomal regions are present in more than 2 copies per cell, resulting in increased expression of genes within these amplified regions. These amplification events typically provide selective growth advantages to cells through increased expression of specific oncogenes (5–7) that act to promote growth and/or survival pathways. In addition to the biological importance of these amplification events, there is evidence indicating that gene amplification can provide potential targets for cancer chemotherapy. For example, ERBB2 amplification serves as a valuable target for treatment of breast cancers with the monoclonal antibody trastuzumab (8, 9).

In the alveolar subtype of rhabdomyosarcoma (RMS), characteristic 2;13 or 1;13 chromosomal translocations generate PAX3-FOXO1 or PAX7-FOXO1 fusions. In addition to these fusions, DNA amplification events occur in a sizable subset of fusion-positive (FP) RMS tumors (10–13). One common amplification event in FP RMS involves the 12q13-q14 chromosomal region and occurs preferentially in the PAX3-FOXO1–positive subset. In these FP RMS cases, this amplicon recurrently involves a region spanning more than 20 genes and is associated with a poor outcome (10, 11). A similar 12q13-q14 amplicon has also been found in other tumor categories, such as carcinomas (including lung adenocarcinoma [LUAD]), sarcomas (including liposarcoma [LPS]), and brain tumors (including glioblastoma multiforme [GBM]) (14, 15). In past studies, the oncogenic effect of this 12q13-q14 amplicon has usually been attributed to increased copy number and overexpression of CDK4, a gene within this amplified region encoding a cyclin-dependent kinase that promotes G_1 to S phase cell-cycle progression. However, the role of other coamplified genes in the 12q13-q14 region has not been well studied.

In this manuscript, we provide further insight into the 12q13-q14 amplicon in FP RMS by comparing copy number and gene expression involving the 12q13-q14 chromosomal region across several cancer types using high-resolution SNP array and RNA-Seq data. This focused analysis allowed comparison and identification of the amplified regions that are common among these multiple tumor categories. Furthermore, our analysis also identified a segment of the 12q13-q14 region that is uniquely and recurrently amplified in FP RMS tumors. Based on these findings, we focused on serine hydroxymethyltransferase 2 (SHMT2), a gene within this unique region that exhibits high expression levels in both FP RMS tumors and cell lines harboring this amplicon. Using RMS cell models, we investigate the role of SHMT2 as an oncogenic driver and as a potential target for treatment of amplicon-positive FP RMS.

Authorship note: THN and PLV contributed equally to this work.
Conflict of interest: FGB holds ownership interest in Abbott Laboratories, Baxter International, Danaher Corp., Edwards Lifesciences, Eli Lilly, Johnson & Johnson, Laboratory Corporation of America, UnitedHealth Group, and Varian Medical Systems.

Submitted: March 11, 2020; **Accepted:** June 16, 2021; **Published:** August 2, 2021.
Reference information: *J Clin Invest*. 2021;131(15):e138022.
https://doi.org/10.1172/JCI138022.

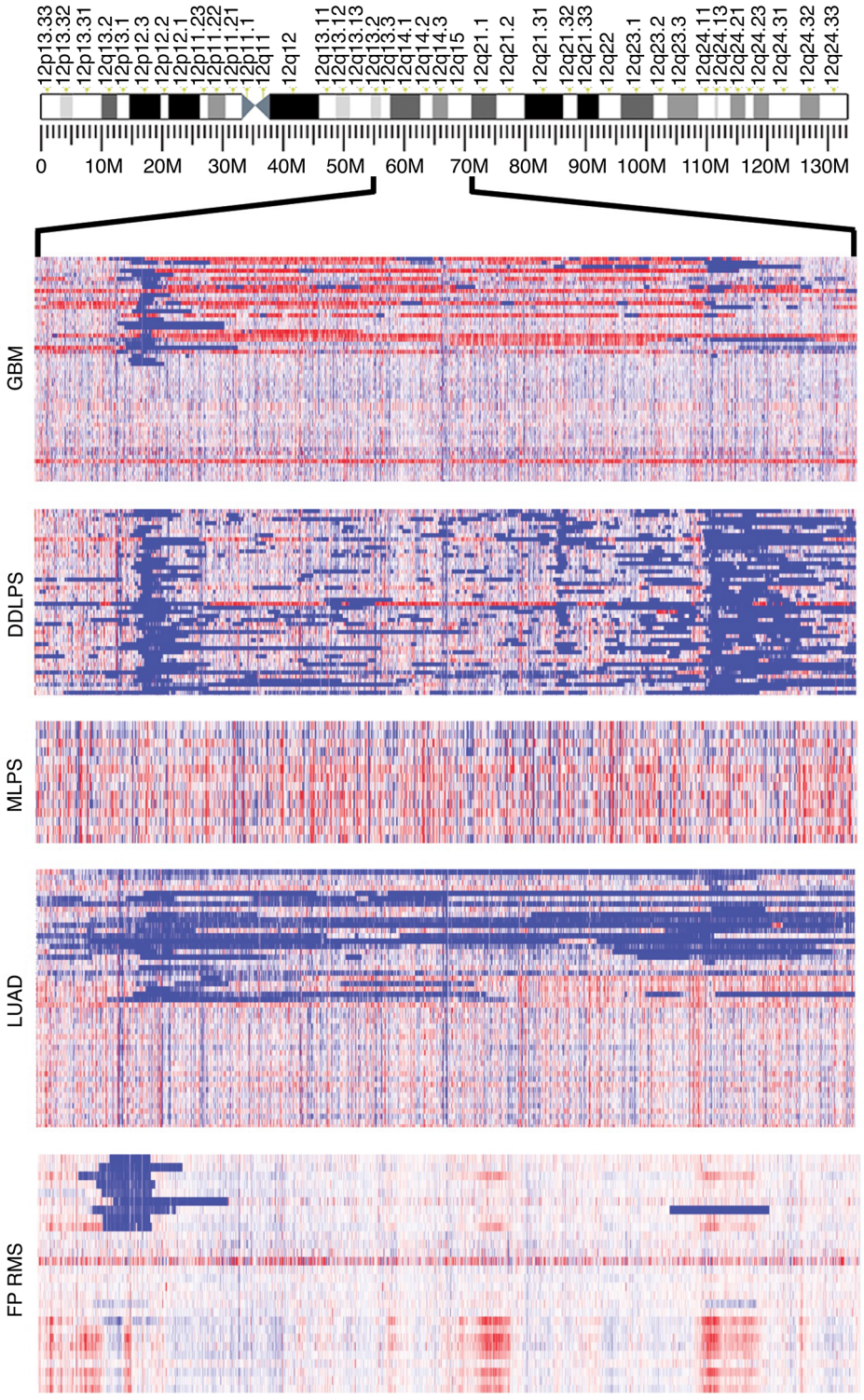

Figure 1. Amplicon distribution in the 12q13-q15 region across tumor types. The amplicons defined by the Nexus SNP-FASST2 algorithm are shown in a subset of amplicon-positive and amplicon-negative samples for each tumor type. Blue represents copy number gains, while red represents losses in the region.

Results

Initial analysis of the 12q13-q14 region. In an initial low-resolution view of chromosome 12 copy number, amplicon-positive and amplicon-negative samples were identified in each tumor category using the criteria described in Methods (Figure 1). We focused on focal amplification events in the 12q13-q14 chromosomal region in the FP RMS, GBM, LUAD, and dedifferentiated LPS (DDLPS) categories. The frequency of 12q13-q14 amplification in each tumor type was as follows: FP RMS (32%), GBM (17%), LUAD (5%), and DDLPS (90%) (Table 1). For the LPS category, the myxoid LPS subtype (MLPS), which is generally not amplified in this region, was used to provide a sufficient number of amplicon-negative LPS cases for comparison with the amplicon-positive DDLPS cases.

This low-resolution analysis of 12q13-q14 amplification identified genomic features that differ among the tumor categories. For DDLPS, most cases had coamplification of the 12q15 region with an intervening nonamplified region. In contrast, GBM had deletion events adjacent to these amplification events. As another variation, the amplicons in LUAD often extended from the 12q13-q14 region through the 12q15 region and further to the 12q21 region. Among these 4 tumor types, FP RMS was distinguished by the presence of focal 12q13-q14 amplification without a high frequency of 12q15 coamplification, adjacent deletion, or elongated amplicons. In this study, we limited our subsequent characterization to amplification of the 12q13-q14 region due to its specificity to FP RMS samples.

Copy number analysis. We next developed a statistical approach to defining the common 12q13-q14 amplification events in RMS, GBM, LUAD, and LPS. In contrast to approaches that only determine the minimal common amplified region, we wanted to statistically define a high-confidence region of amplification for each cancer type. We divided the chromosomal regions of interest into multiple segments, where the segment length was chosen to provide a sufficient number of probes to reliably determine the copy number of each segment and detect statistically relevant differences in copy number between amplicon-positive and amplicon-negative samples. The overall region under analysis was chosen such that copy number changes in amplified cases returned back to baseline within the outermost segments of the region or at least were consistently scored as not significantly amplified based on the filtering criteria described below.

Table 1. Categorization of the number of samples based on copy number status in each tumor type

Amplicon	Tumor type	Amplicon-positive	Amplicon-negative	Low gain	Whole chromosome gain	Total	Platform
12q13-q14	FP RMS	9	19	0	0	28	Omni 2.5M
12q13-q14	GBM	25	100	12	13	150	SNP 6.0
12q13-q14	LUAD	25	337	46	68	476	SNP 6.0
12q13-q14	DDLPS	45	2	2	1	50	SNP 6.0
12q13-q14	MLPS	1	16	3	4	24	SNP 6.0

To examine amplification within the 12q13-q14 region in the 4 cancer categories, a 6 Mb region from 56 Mb to 62 Mb was split into 60 segments, each measuring 100 kb in length (Figure 2). Box plots were used to visualize the distribution of copy number calls in each genomic segment in each of the tumor categories. Each box plot showed the variation of probe median data at each genomic segment in either amplified or nonamplified cases and thereby permitted visualization of the differences in copy number between the 2 groups. Statistical analyses of these differences then allowed for determination of which intervals had a statistically significant difference in copy number between amplified and nonamplified cases and thus delineated a high-confidence region of amplification for each tumor category.

Our analysis of the 12q13-q14 amplification in FP RMS, GBM, LUAD, and DDLPS revealed high-confidence regions of amplification ranging from 0.5 Mb in GBM to 1.6 Mb in LUAD, as summarized in Figure 3A. These high-confidence regions of amplification in each tumor category show a substantial separation between the median copy number of amplicon-positive samples and that of amplicon-negative samples, confirming the significant copy number gains in these tumors (Figure 2). Of note, there were 2 high-confidence regions of amplification in LUAD that were separated by a small (0.1 Mb) intervening nonamplified region (Figure 2 and Figure 3A). In our comparison of these amplification events, we observed an overlap of 0.2 Mb across the 4 tumor categories (Figure 3A), which spanned from 58.0 Mb to 58.2 Mb and contained 15 genes (DTX3, ARHGEF25, SLC26A10, B4GALNT1, OS9, AGAP2-AS1, AGAP2, TSPAN31, CDK4, MARCH9, CYP27B1, METTL1, EEF1AKMT3, TSFM, and AVIL). In addition, there was a 0.1 Mb region of amplification common to GBM and RMS and a 0.2 Mb region of amplification common to GBM, DDLPS, and LUAD. Finally, our results demonstrate that the amplicons in DDLPS and LUAD extended further distally, while the amplicon in FP RMS extended further proximally. In particular, there was a 0.5 Mb amplified region that was specific to FP RMS and a 0.9 Mb amplified region that was specific to LUAD. Though copy number in most tumors returned to background levels near the endpoints of the 6 Mb region, a subset of tumors demonstrated copy number changes in these regions. For example, a subset of LUAD cases showed copy number gains on either side of the demarcated common amplified region, as suggested by our initial low-resolution analysis of these cases (Figure 1). This finding is reflected in the wide distribution of probe median values above 0 in the amplicon-positive box plots and provides evidence of intertumor heterogeneity (Figure 2). In contrast, we observed that GBM was the only tumor category in which a deletion event followed the amplification event (Figure 1). This feature is demonstrated by the wide distribution of probe median values below 0 in the amplicon box plots and extends distally from the amplified region to beyond the end of the analyzed region (Figure 2).

Expression of genes in the amplified region. To study the association of amplification and expression of genes in this region, we analyzed RNA-Seq data to determine whether genes contained in the amplification region are overexpressed in amplified cases. We analyzed 48 genes in and around the 12q13-q14 amplicons for differential gene expression between amplified and nonamplified samples. As with copy number analysis, box plots were used to visualize the distribution of normalized gene expression between amplified and nonamplified cases for each gene within each tumor category (Figure 3B and Supplemental Figure 1; supplemental material available online with this article; https://doi.org/10.1172/JCI138022DS1). The results show that 14 genes in FP RMS, 18 genes in GBM, 15 genes in LUAD, and 15 genes in DDLPS were significantly overexpressed in amplified samples. Of note, OS9, TSPAN31, CDK4, CYP27B1, METTL1, EEF1AKMT3, and TSFM were overexpressed in amplicon-positive samples in all 4 cancer categories and contained within the 0.2 Mb commonly amplified region. Two genes (CTDSP2 and ATP23) were preferentially overexpressed in amplified cases of GBM, LUAD, and LPS and contained within the region specifically amplified in these 3 tumor categories. Furthermore, there were 4 genes (NEMP1, NAB2, SHMT2, and R3HDM2) that were differentially expressed only in amplified FP RMS and map to the FP RMS–specific amplified region. In subsequent experiments, we focused on understanding the biological significance of amplification and altered expression of these genes within this 0.5 Mb RMS-specific region.

The 12q13-q14 amplicon and its overexpressed genes in RMS cell lines. We first sought to identify cell line models that are relevant to 12q13-q14 amplicon-positive FP RMS. We screened for the 12q13-q14 amplicon in a panel of 11 RMS cell lines, including 3 fusion negative (FN) (Rh6, RD, SMS-CTR), 1 PAX7-FOXO1 positive (CW9019), and 7 PAX3-FOXO1 positive (Rh3, MP4, NIH-RMS-097, Rh5, Rh28, Rh30, and Rh41), by quantifying the relative copy number of CDK4 and SHMT2 compared with control centromeric chromosome 12-specific regions. Only genomic DNA from Rh30 cells exhibited significantly higher CDK4 and SHMT2 copy numbers, which were 7-fold and 8-fold higher, respectively, than the corresponding copy numbers in the other RMS cell lines (Figure 4A). This finding is corroborated by our previous in situ hybridization study showing that CDK4 is specifically amplified in Rh30 cells (16). These results therefore

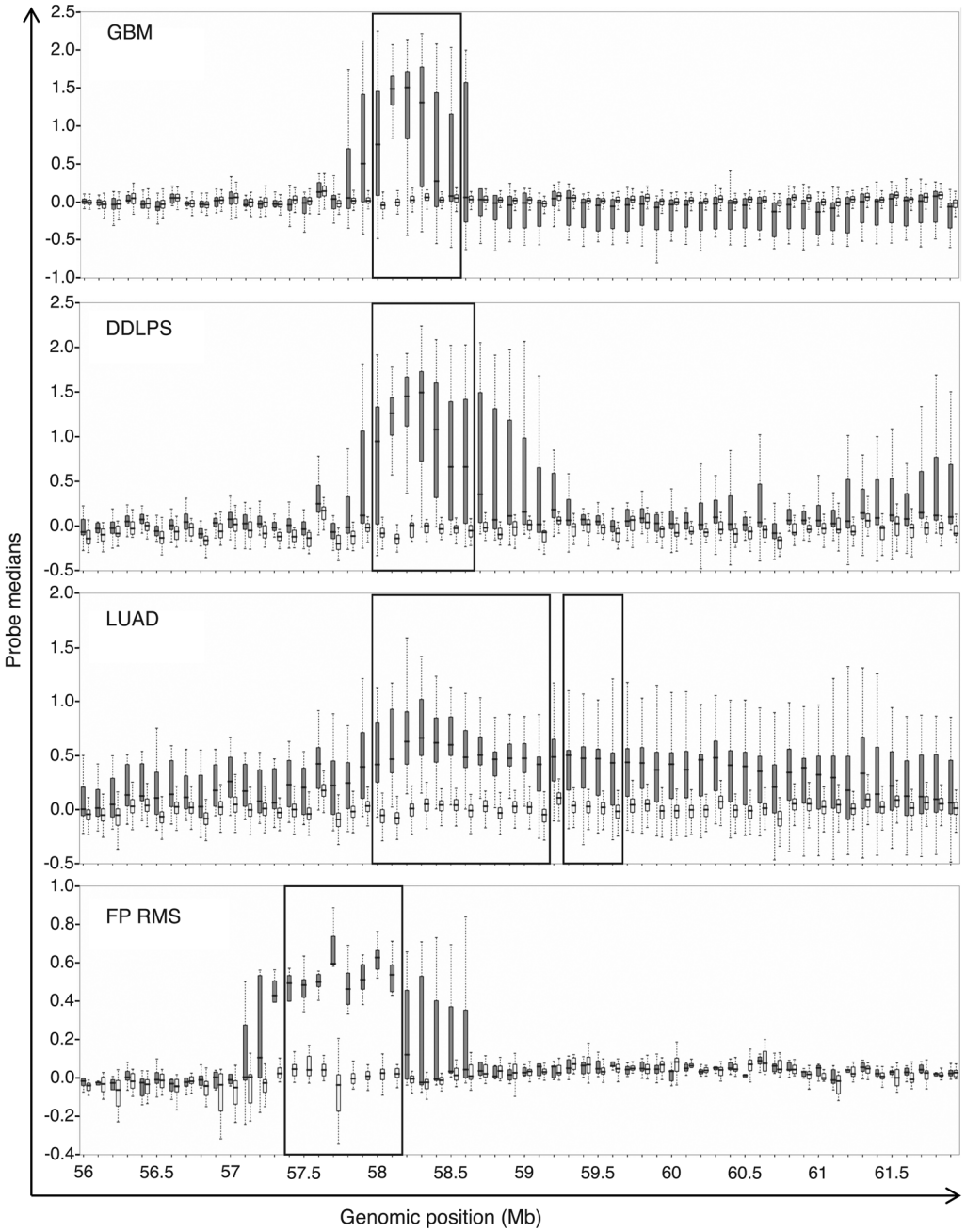

Figure 2. Location of the 12q13-q14 amplicon across tumor types. A 6 Mb region was split into 100 kb intervals and analyzed for significant differences in copy number between amplicon-positive samples (gray) and amplicon-negative samples (white). The regions indicated with black rectangles represent high-confidence regions of amplification as defined by copy number changes with Bonferroni's corrected *P* values ≤ 0.05 and fold changes ≥ 1.4.

indicate that Rh30 harbors the 12q13-q14 amplicon and constitutes a relevant FP RMS cell model for this amplicon.

We next investigated mRNA expression of NEMP1, NAB2, SHMT2, and R3HDM2 in these RMS cell lines. SHMT2 and NAB2 showed significantly higher mRNA expression in Rh30 compared with the amplicon-negative RMS lines (Figure 4B), whereas NEMP1 and R3HDM2 did not exhibit increased expression in Rh30 cells. For the 2 genes overexpressed in Rh30 cells at the RNA level, further analysis of protein expression found that only SHMT2 had a consistently higher protein expression level in Rh30 than in the amplicon-negative RMS cell lines (Figure 4C). Based on these findings, we proceeded to focus on SHMT2 and investigated the potential role of this protein in regulating the oncogenic phenotype of FP RMS.

Correlative studies of SHMT2 expression in FP RMS. We further studied the relationship between SHMT2 amplification and expression in 13 patient-derived xenograft (PDX) samples propagated from FP RMS tumors. Our quantitative PCR (qPCR) assay of genomic DNA from these PDX samples showed that 3 of these samples have more than a 2-fold increase in SHMT2 copy number (Figure 5A), indicating the presence of SHMT2 amplification in these tumors. We then examined RNA and protein expression of SHMT2 in these samples. The SHMT2 mRNA levels were significantly higher in the 3 SHMT2-amplified tumors compared with the nonamplified samples (Figure 5B). Similarly, Western blotting showed that the SHMT2 protein levels were also significantly higher in the SHMT2-amplified tumors (Figure 5, C and D). These data indicate that high

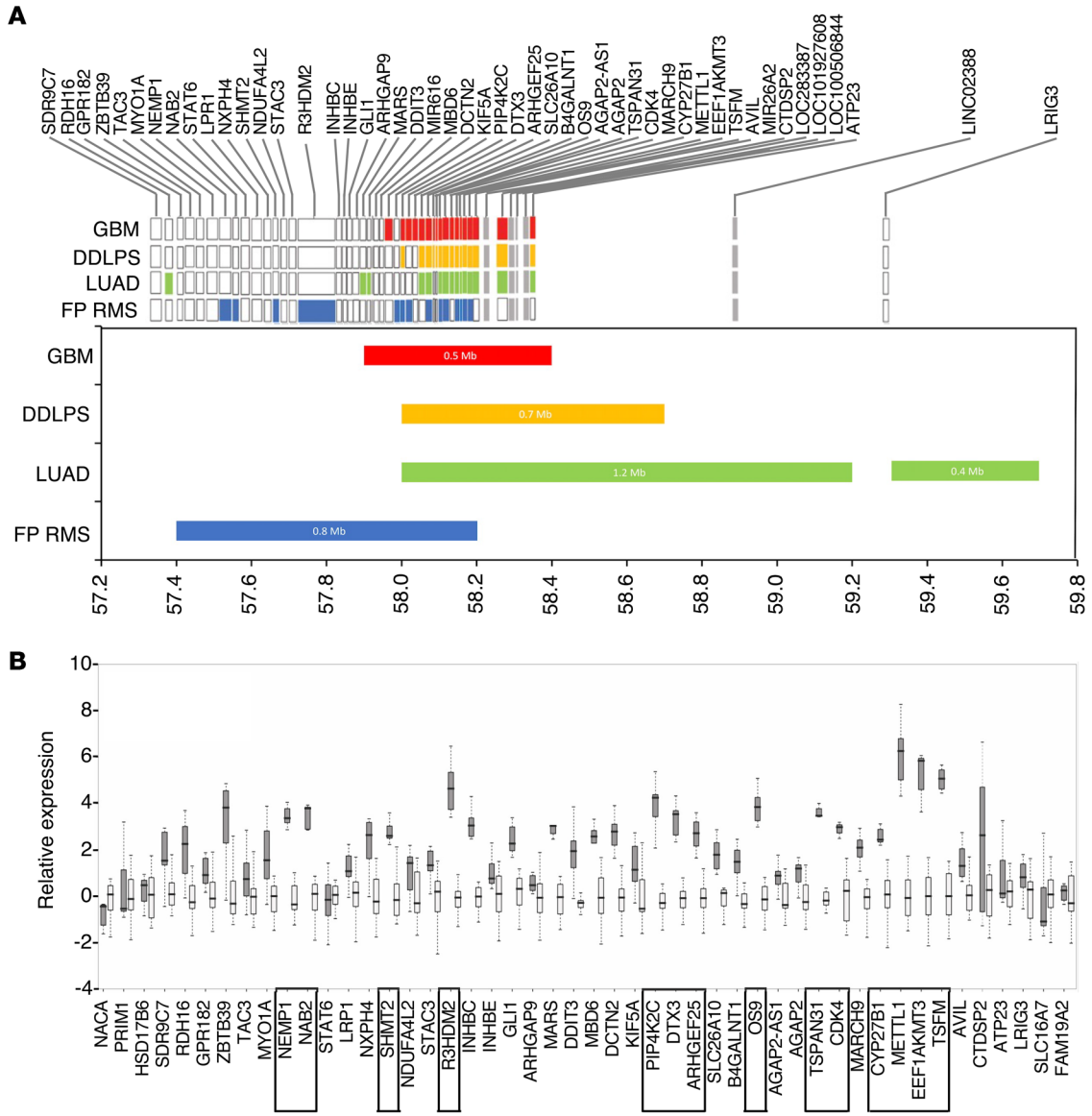

Figure 3. Distribution of 12q13-q14 amplicons across cancer types and expression in FP RMS. (**A**) Summary of the sizes, distributions, and expression consequences of 12q13-q14 amplicons in each tumor type. The large colored rectangles correspond to the high-confidence regions of amplification, which are the genomic regions that are significantly and highly amplified in amplicon-positive samples, as described in Figure 2. Genes that are significantly and highly overexpressed in amplicon-positive samples were determined as described in Figure 3B and are shown as small colored rectangles. Gray bars indicate that there was insufficient RNA-Seq data for the corresponding genes. (**B**) Expression levels of genes from the 12q13-q14 region in FP RMS tumors. Genes in and around the 12q13-q14 amplified region were analyzed for significant differences in gene-expression levels between amplicon-positive (gray) and amplicon-negative (white) samples. Genes that had Bonferroni's corrected *P* values ≤ 0.05 and fold changes ≥ 2.0 are indicated with black rectangles.

SHMT2 mRNA and protein expression are associated with amplification in FP RMS tumor samples.

To investigate the impact of SHMT2 expression on patient survival, we utilized a published data set of expression microarray and outcome data from 34 FP RMS patients (17). These patients were stratified into "low" and "high" SHMT2 expression based on the median expression levels of SHMT2 mRNA (Supplemental Figure 2). In this FP RMS patient cohort, high expression of SHMT2 was significantly correlated with worse survival ($P = 0.021$). This result is consistent with our previous finding that amplification of the 12q13-q14 chromosomal region is associated with a poor outcome in FP RMS (11).

Knockdown of SHMT2 suppresses cell growth and tumor formation. The SHMT2 protein is a mitochondrial serine hydroxymethyltransferase that functions in the synthesis of glycine and serine and in 1-carbon metabolism to provide building blocks for the synthesis of nucleotides, polyamines, amino acids, creatine, and phospholipids (18). To examine the biological role of SHMT2 in FP RMS oncogenesis, we first employed shRNA expression constructs to specifically reduce SHMT2 expression in amplicon-positive Rh30 cells. Two independent shRNAs efficiently inhibited the expression of SHMT2 at both mRNA (Figure 6A) and protein (Figure 6B) levels, while not significantly affecting the expression of SHMT1, which encodes a related cytoplasmic protein (Figure 6B). To determine whether the

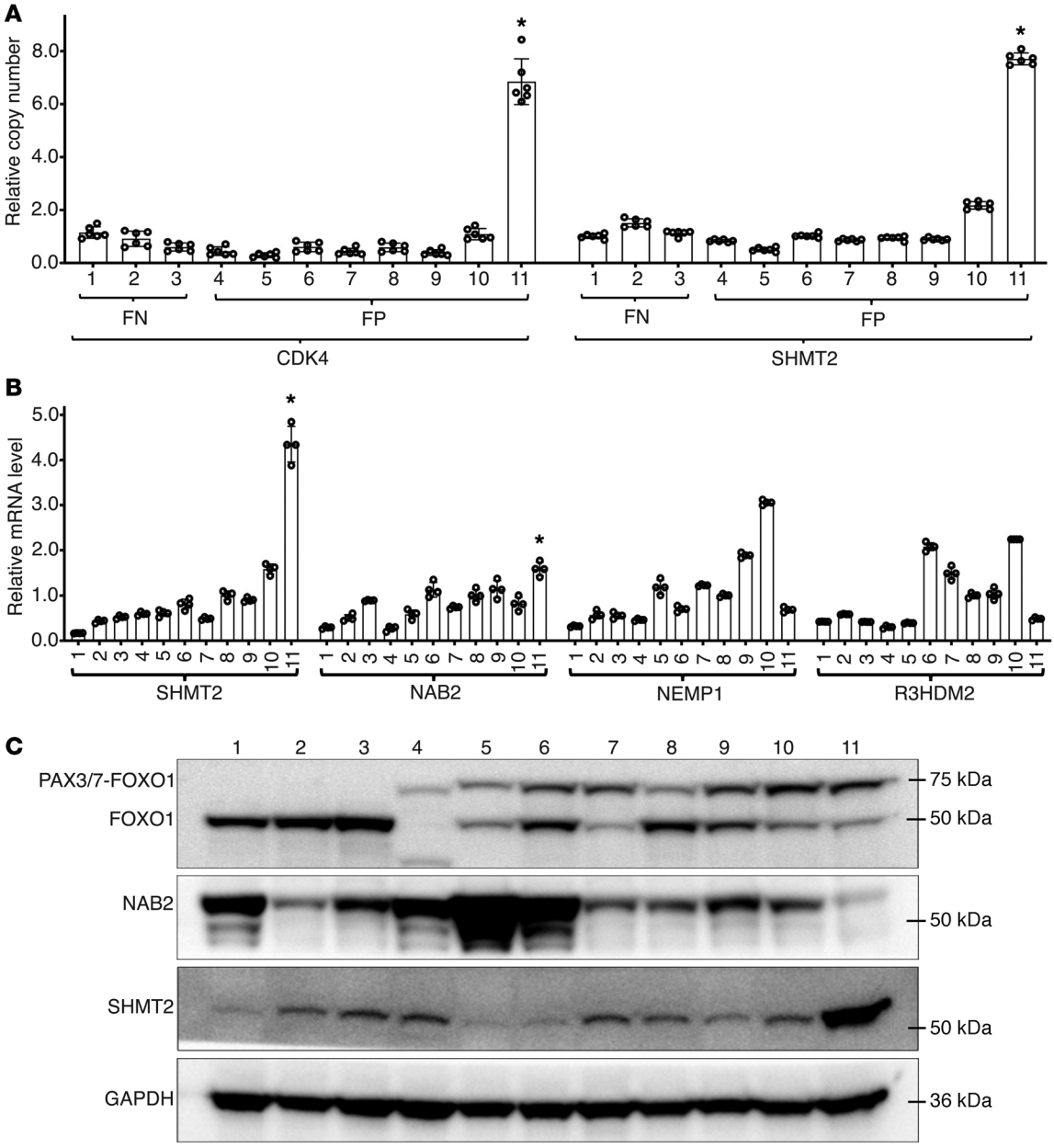

Figure 4. Amplification and expression of the 12q13-q14 region in RMS cell lines. Cell lines are indicated by numbers: FN: 1-Rh6, 2-RD, 3-SMS-CTR; FP: 4-CW9019, 5-MP4, 6-RMS-097, 7-Rh3, 8-Rh5, 9-Rh28, 10-Rh41 and 11-Rh30 (all were PAX3-FOXO1-positive except for CW9019, which is PAX7-FOXO1-positive). (**A**) Screening for the 12q13-q14 amplicon in RMS cell lines. Graph shows relative copy numbers of CDK4 and SHMT2 in genomic DNA quantified by qPCR and normalized against the centromeric D12Z3. RD cells were used as a negative control in which copy numbers of CDK4 and SHMT2 were set at 1.0. Data are represented as mean ± SD of 6 technical replicates from 2 biological replicates. Statistical analysis of copy numbers in Rh30 versus the other lines was performed using Student's *t* test. $^*P < 0.01$. (**B**) mRNA expression of NEMP1, NAB2, SHMT2, and R3HDM2. Graph shows relative mRNA expression quantified by quantitative reverse-transcriptase PCR (qRT-PCR). GAPDH was used for normalization. Data are represented as mean ± SD of 4 replicates. Statistical analysis of expression differences in Rh30 versus the other lines was performed using Student's *t* test. $^*P < 0.05$. (**C**) Protein expression of SHMT2, NAB2, FOXO1, and PAX3/7-FOXO1 in cell lines. The immunoblot was probed with SHMT2 antibody, stripped, and reprobed with other antibodies. Relevant areas of the blot are shown. GAPDH was used as a loading control.

shRNA-mediated knockdown of SHMT2 results in suppression of SHMT2 functional activity, we measured the cellular level of NADPH, which is one of the products of the 1-carbon metabolism process (19). This experiment demonstrated that cellular levels of NADPH were significantly reduced in SHMT2-knockdown Rh30 cells (Figure 6C), indicating that decreased SHMT2 expression mediated by the shRNAs effectively suppresses SHMT2 function.

We next employed a series of in vitro and in vivo assays to study the oncogenic role of SHMT2 in FP RMS. Both shRNAs suppressed Rh30 cell growth and proliferation compared with the control vector, as measured by real-time monitoring of cell growth (Figure 6D) and clonogenic assays (Figure 6E and Supplemental Figure 3A). Furthermore, a role for SHMT2 in FP RMS oncogenesis is shown by our finding of SHMT2 knockdown leading to a strong reduction in focus

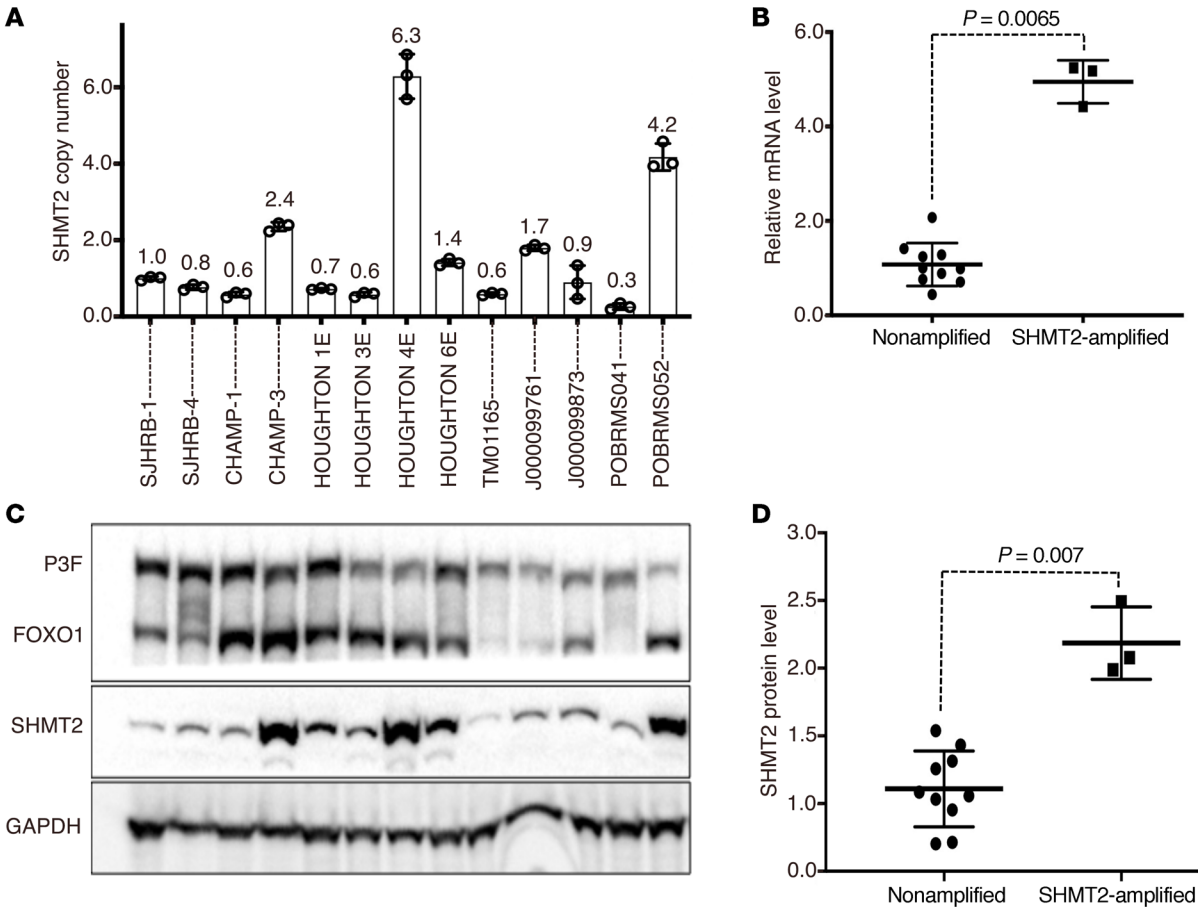

Figure 5. Amplification and expression of SHMT2 in FP RMS PDX tumors. (**A**) SHMT2 amplification in a set of 13 FP RMS PDX tumors. Graph shows relative copy numbers of SHMT2 in genomic DNA quantified by qPCR and normalized against the centromeric D12Z3. Data are represented as mean ± SD of 3 replicates. (**B**) SHMT2 mRNA expression. Tumors are categorized into 2 groups based on the SHMT2 copy number: amplification negative (SJHBR1, SJHBR4, CHAMP1, HOUGHTON1E, HOUGHTON3E, HOUGHTON6E, TIM01165, J000099761, J000099873 and POBRMS041) with a copy number less than 2 and amplification positive (11-CHAMP3, HOUGHTON4E, and 13-POBRMS052) with a copy number greater than 2. A distribution plot shows relative mRNA expression quantified by qRT-PCR in the 2 groups. GAPDH was used for normalization of RNA-expression data. Each point represents the mean expression value of 3 technical replicates of each tumor. (**C**) SHMT2 protein expression. Protein expression of PAX3-FOXO1 (P3F), FOXO1, SHMT2, and GAPDH (loading control) was assessed in PDX tumors by immunoblotting. (**D**) Quantitation of SHMT2 protein level. Protein bands were inverted and quantified by ImageJ. Relative protein levels were expressed as a ratio of the band intensities of SHMT2 and GAPDH. Distribution plot shows the relative SHMT2 protein levels in the 2 groups. Statistical analysis of expression differences between the 2 groups in **B** and **D** was performed using Student's *t* test (2 tailed, nonparametric, and nonpairing) in Prism 8.

formation of Rh30 cells (Figure 6F and Supplemental Figure 3B) and a slower growth of xenograft tumors in mice (Figure 6, G and H, and Supplemental Figure 4A). Further analysis revealed that, among the 5 tumors that developed from shRNA-expressing cells (Figure 6G), 3 exhibited strong growth suppression while 2 displayed either more modest (tumor 1) or no obvious (tumor 5) effect (Supplemental Figure 4A). Quantification of mRNA expression in these tumors showed that tumors 2 to 5 still exhibited significant suppression of SHMT2 expression (>70% knockdown), whereas tumor 1 had much less SHMT2 suppression (~32%) compared with control tumors (Supplemental Figure 4B). While this finding explains the larger size of tumor 1, it remains unclear why the reduced SHMT2 expression in tumor 5 did not suppress tumor growth.

Although SHMT1 and SHMT2 localize and function in different cellular compartments, these 2 proteins have similar enzymatic activity (20). We determined whether increased SHMT1 expression could compensate for the loss of SHMT2 expression by overexpressing SHMT1 in Rh30 cells with depleted SHMT2 (Supplemental Figure 5A). In assays of cell growth, SHMT1 overexpression did not rescue the suppressive phenotype resulting from SHMT2 loss in Rh30 cells (Supplemental Figure 5B). This finding is consistent with previous reports that expression of SHMT2, but not SHMT1, is important for cell growth and proliferation of lymphoma (21, 22), hepatocellular carcinoma (23), and colorectal cancer cells (24).

To further understand the biological effect of SHMT2, we asked whether SHMT2 is also required for growth of other FP RMS cells that do not harbor the 12q13-q14 amplicon and express low levels of SHMT2. In experiments similar to those described above, we observed a growth-suppressive effect of shRNA-mediated decreases of SHMT2 expression in Rh41 (Supplemental Figure 6) and Rh5 (Supplemental Figure 7) cells measured by real-time growth and clonogenic and focus formation assays. These results are consistent with the premise that SHMT2 is generally required for FP RMS cell growth regardless of the SHMT2 expression level.

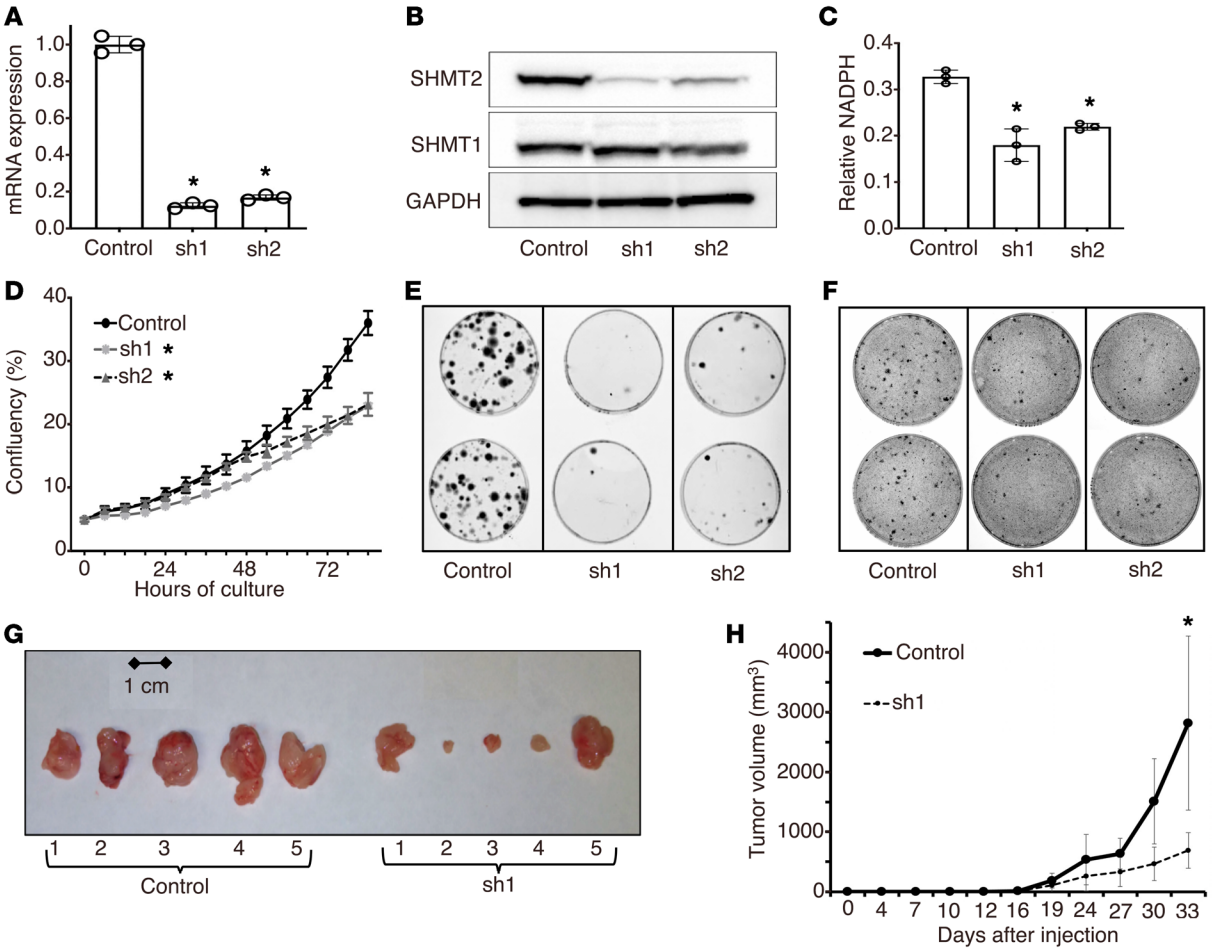

Figure 6. Effect of SHMT2 knockdown on Rh30 cell growth and transformation. (**A**) Quantitation of SHMT2 mRNA expression by qRT-PCR in control and SHMT2 shRNA-expressing Rh30 cells. GAPDH was used for normalization. Data are represented as mean ± SD of 3 replicates. (**B**) Western blot analysis of SHMT1 and SHMT2 expression in control or shRNA-expressing cells. GAPDH was used as loading control. (**C**) Measurement of NADPH cellular levels in control and shRNA-expressing cells. Data are represented as mean ± SD of 3 replicates. (**D**) IncuCyte growth assay. Data are represented as mean confluence ± SEM of 4 different wells. (**E**) Clonogenic assay: 360 cells were seeded in 6 cm dishes, cultured for 3 weeks, then fixed and stained with Giemsa. (**F**) Focus formation assay: 500 cells were cocultured with 2×10^5 NIH 3T3 fibroblasts in 6-well dishes for 3 weeks, then fixed and stained with Giemsa. (**G**) Intramuscular xenograft tumor formation of Rh30 cells. All tumors (5 mice per group) were excised when the largest tumor reached the maximum size permitted. (**H**) Xenograft tumor growth. Tumor sizes were measured twice weekly, and tumor volume was calculated as (width^2 ×length)/2. Data are shown as mean volume ± SD of 4 mice per group. For **A** and **C**, Dunnett's multiple comparisons test was used for statistical analysis. *$P < 0.0001$ (**A**); *$P < 0.01$ (**C**). For **D**, ANOVA tests (corrected for multiple comparisons using the Šidák-Bonferroni method) were performed for the last 6 time points. *$P < 0.05$, adjusted. For **H**, Student's *t* test (2 tailed, type 2) was used for statistical analysis. *$P < 0.05$. Experiments in **A**, **B**, **D**, **E**, and **F** were repeated at least 3 times, and representative data are shown. Results shown in **G** and **H** were derived from separate independent experiments.

Overexpression of SHMT2 stimulates cell growth and tumor formation. We next investigated the effect of SHMT2 overexpression on growth and proliferation of Rh41 and Rh5, 2 FP RMS cell lines that express relatively low SHMT2 levels compared with Rh30 cells (Figure 4C). Transduction of a SHMT2 cDNA expression construct into these cell lines resulted in increased SHMT2 expression, which was still lower than the level in Rh30 cells (Figure 7A and Supplemental Figure 9A). To confirm that the exogenously expressed protein was functional, we again monitored NADPH levels as a downstream readout of SHMT2 activity. Rh41 cells expressing increased SHMT2 levels had a significantly higher cellular level of NADPH, as compared with control cells expressing an empty vector, indicating that the overexpressed SHMT2 protein was enzymatically active (Figure 7B). Using a real-time cell growth assay, we found that SHMT2 overexpression promoted growth and proliferation of Rh41 (Figure 7C) and Rh5 (Supplemental Figure 9B) cells. Furthermore, the increase in SHMT2 expression enhanced clonogenic growth and focus formation of Rh41 (Figure 7, D and E, and Supplemental Figure 8, A and B) and Rh5 (Supplemental Figure 9, C–F) cells. To extend these findings to in vivo tumorigenesis, we performed orthotopic injections of Rh41 cells into mice and found that SHMT2-overexpressing Rh41 cells formed tumors earlier than control Rh41 cells and that these tumors were larger in size (Figure 7, F and G). These data indicate that increased SHMT2 expression promotes cell growth, oncogenic transformation, and tumorigenesis.

High SHMT2-expressing RMS cells are less sensitive to the SHMT inhibitor SHIN1. Since our data indicate that SHMT2 has a growth-stimulating effect in FP RMS cell models, we explored

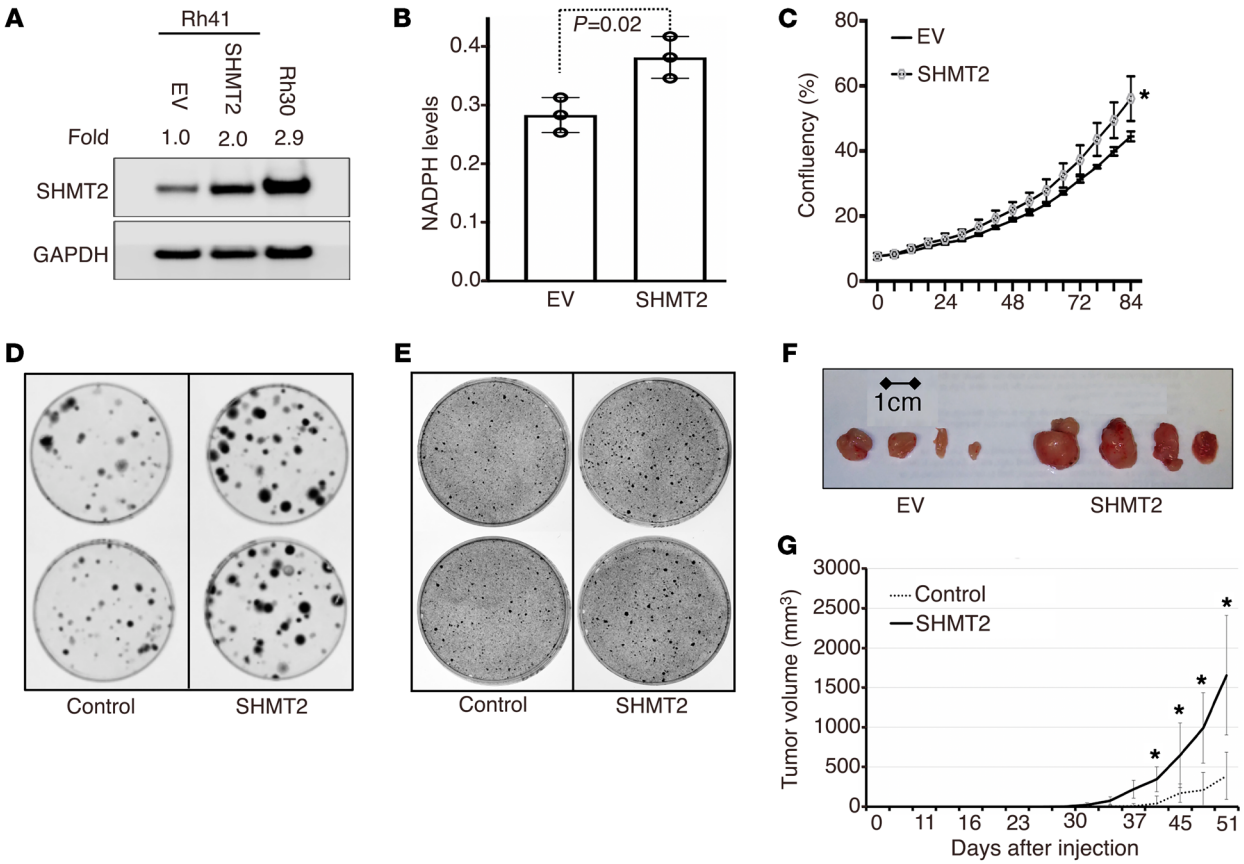

Figure 7. Effect of SHMT2 overexpression on Rh41 cell growth and transformation. (**A**) SHMT2 protein expression in control or SHMT2-expressing Rh41 cells. Rh30 cells were used for comparison, and GAPDH was used as a loading control. Expression was quantified as described in Figure 5. (**B**) Measurement of NADPH levels in control or SHMT2-expressing Rh41 cells. Total unfiltered protein concentrations were used for normalization. Data represent mean ± SD of 3 replicates. Student's *t* test was used for statistical analysis. (**C**) IncuCyte growth assay. Data are represented as mean ± SEM of 4 different wells. Multiple *t* tests (corrected for multiple comparisons using the Šidák-Bonferroni method) were performed for the last 6 time points to assess the significance in growth differences. **P* < 0.05, adjusted. (**D**) Clonogenic assay. 360 cells were seeded in 6 cm dishes, cultured for 3 weeks, then fixed and stained with Giemsa. (**E**) Focus formation assay: 500 cells were cocultured with 2 × 10^5 NIH 3T3 fibroblasts for 4 weeks, then fixed and stained with Giemsa. (**F**) Intramuscular xenograft tumor formation of control or SHMT2-expressing Rh41 cells. All tumors (4 mice per group) were excised when the largest tumor reached the maximum size permitted. (**G**) Xenograft tumor growth in mice. Tumors (7 mice per group) were measured twice weekly, and data are expressed as mean volume ± SD. Student's *t* test was performed to determine the significance of growth differences between the groups. **P* < 0.05. Experiments shown in **A**, **C**, **D**, and **E** were repeated at least 3 times, and representative data are shown. Results shown in **F** and **G** were derived from separate independent experiments.

the possibility of targeting SHMT2 using small-molecule inhibitors. We first examined the effect of SHIN1, a recently reported small molecule that specifically binds to and inhibits SHMT enzymatic activity through a single enantiomer-enzyme interaction (21). A real-time growth assay of Rh30 cells treated with various concentrations of SHIN1 revealed a growth-suppressive effect at SHIN1 concentrations higher than 12.5 μM (Figure 8A); the IC_{50} of SHIN1 in Rh30 cells was determined to be 71 μM. In a comparison of the effect on multiple FP RMS cell lines, the SHIN1 IC_{50} was 3- to 5-fold higher in Rh30 cells than in FP RMS cell lines without SHMT2 amplification (Figure 8B). Based on these findings, we reasoned that the SHMT2 expression levels in RMS cells might influence their sensitivity to the inhibitor.

To test the hypothesis that SHMT2 levels affect susceptibility to SHIN1, we compared the effect of SHIN1 on Rh30 cells expressing a SHMT2 shRNA or control construct. At the concentration of 10 μM, SHIN1 had no effect on control Rh30 cells, but exhibited a strong inhibitory effect on SHMT2-depleted cells; this effect was further magnified at a higher dose of SHIN1 (50 μM; Figure 8C). Overall, the SHIN1 IC_{50} in SHMT2-depleted Rh30 cells was reduced significantly compared with that in the control cells (26 vs. 71 μM; Figure 8D). Similar results were obtained when depleting SHMT2 in Rh41 and Rh5 cells (Figure 8D). To further understand the connection between the SHMT2 expression level and response to SHIN1, we examined the SHIN1 IC_{50}s in Rh41 and Rh5 cells transduced with an empty or SHMT2 expression vector. In conjunction with the increase in SHMT2 expression in these cells (Figure 7A and Supplemental Figure 9A), we observed a modest increase in SHIN1 IC_{50} in cells transduced with the SHMT2 expression construct (Figure 8E). The combined findings in SHMT2-depleted and SHMT2-augmented cells clearly indicate that the SHMT2 expression level inversely affects the sensitivity of RMS cells to SHIN1. We propose that this inverse relationship results from the use of a drug that directly targets SHMT2 and suggest that this direct targeting approach is not suitable for treating 12q13-q14 amplicon-positive FP RMS tumors.

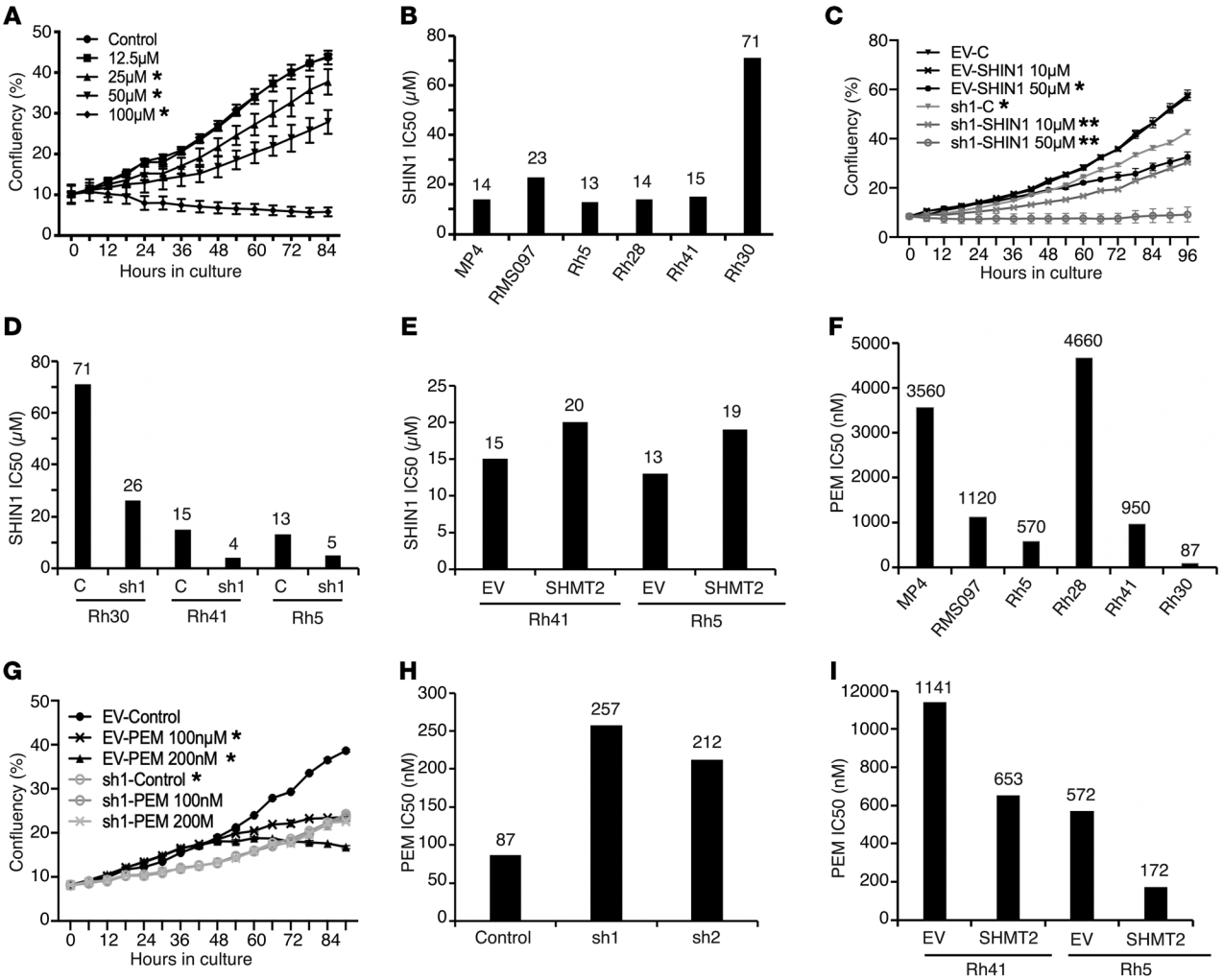

Figure 8. Effect of SHMT2 inhibitors on RMS cell growth. (**A**) IncuCyte assay of SHIN1 effect on cell growth. Rh30 cells were treated with indicated SHIN1 concentrations. Data are represented as mean confluence values ± SEM of 4 well replicates. (**B**) IC_{50} of SHIN1 in RMS cell lines. Cells (4 wells per dose) were treated with control (DMSO) or 2-fold serial dilutions of SHIN1 (from 1.56 to 100 μM). Mean confluence values at 96 hours were used to calculate IC_{50}. (**C**) Effect of SHIN1 on growth of SHMT2 shRNA-expressing Rh30 cells. Assay was performed as described for **A**. (**D**) IC_{50} of SHIN1 in Rh30, Rh41, and Rh5 cells expressing control or SHMT2 shRNA. Assay was performed as described in **B**. (**E**) IC_{50} of SHIN1 in Rh41 and Rh5 cells expressing control or SHMT2 construct. Assay was performed as described for **B**. (**F**) IC_{50} of PEM in RMS cell lines. Assay was performed as described for **B** with PEM concentrations ranging from 50 to 6400 nM. (**G**) Effect of PEM on growth of control or SHMT2 shRNA-expressing Rh30 cells. Cells were treated with indicated PEM concentrations, and growth was monitored as described for **A**. (**H**) IC_{50} of PEM in control or SHMT2 shRNA-expressing Rh30 cells. Assay was performed as described for **F**. (**I**) IC_{50} of PEM in Rh41 and Rh5 cells expressing control or SHMT2 construct. Assay was performed as described for **F**. Experiments shown in **A**, **C**, and **G** were repeated at least 3 times, and ANOVA tests (corrected for multiple comparisons) were performed for the last 6 time points. $^{*}P < 0.05$, adjusted (**A** and **G**); $^{*}P < 0.05$ compared with EV-control (**C**); $^{**}P < 0.05$ compared with sh1-control (**C**).

High SHMT2-expressing RMS cells are more sensitive to the folate inhibitor pemetrexed. Since changes in SHMT2 expression inversely affect the efficacy of a direct-acting inhibitor, we then considered whether an indirect-acting inhibitor might be more efficacious. SHMT2 catalyzes the reversible conversion of serine and tetrahydrofolate (THF) to glycine and 5,10-methylene-THF, providing 1-carbon units (also referred to as methyl groups) for the folate cycle. Since SHMT2 ultimately regulates the production of folate metabolites, we asked whether SHMT2 expression in FP RMS cells might influence cellular sensitivity to folate inhibitors. We first measured the IC_{50} of the folate inhibitor pemetrexed (PEM), which is an FDA-approved drug for treatment of non–small lung cell carcinoma (NSCLC), in our FP RMS cell lines. In contrast to the effect observed with SHIN1 treatment, Rh30 cells were much more sensitive to PEM compared with the other FP RMS lines. In particular, the IC_{50} for PEM in Rh30 cells was 87 nM, whereas the IC_{50} ranged from 6- to 50-fold higher in the 12q13-q14 amplicon-negative FP RMS cell lines (Figure 8F). To corroborate this finding, we also examined the drug sensitivity of an FP RMS line (RMS052) that we recently developed from a SHMT2-amplified PDX tumor (Figure 5). Similarly to Rh30, RMS052 cells expressed a high level of SHMT2 protein compared with nonamplified FP RMS cell lines (Supplemental Figure 10A). Subsequent drug-treatment studies revealed that RMS052 cells were similar to Rh30 in showing a high sensitivity to PEM compared with the other FP RMS lines (Supplemental Figure 10B).

To further elucidate the relationship between SHMT2 expression and cellular response to PEM, we compared the effect of PEM on Rh30 cells expressing control or SHMT2 shRNA. Though growth of control Rh30 cells was significantly affected by treatment with 100 or 200 nM of PEM, growth of SHMT2-depleted Rh30 cells was not significantly affected by these doses of PEM (Figure 8G). In further studies, we found that these cells had a much higher PEM IC_{50} compared with control cells (Figure 8H). To further substantiate this finding, we compared the PEM responsiveness of Rh41 or Rh5 cells transduced with a control or SHMT2-expression construct and found that SHMT2 expression enhanced sensitivity of Rh41 or Rh5 cells to PEM (Figure 8I). These data indicate that RMS cells expressing higher levels of SHMT2 are more sensitive to PEM, suggesting that an approach, such as this folate inhibitor, that targets events downstream of SHMT2 may be useful for treatment of 12q13-q14 amplicon-positive FP RMS tumors.

Since PEM is an approved drug to treat NSCLC patients, we also compared the relative sensitivity of FP RMS and NSCLC cancer cells to this folate inhibitor. Western blotting analysis (Supplemental Figure 11A) revealed that Rh30 expresses significantly higher levels of SHMT2 protein than Rh41 and 6 NSCLC (A549, NCI-H3122, NCI-H226, NCI-H460, NCI-H1299 and NCI-H1993) cell lines that were previously reported to be sensitive to PEM (25). The small cell lung cancer cell line (NCI-H69) was used as a control cell line that is not sensitive to PEM (26). Drug-treatment studies showed that Rh30 cells were at least 3.7-fold more sensitive to PEM when compared with PEM-sensitive lung cancer cell lines (Supplemental Figure 11B). These data suggest that SHMT2-amplified RMS tumors may be more sensitive than NSCLC tumors (without SHMT2 amplification) to PEM treatment and thus the PEM doses currently used for treatment of NSCLC patients may be effective in the treatment of SHMT2-amplified RMS tumors.

Discussion

In this study, we performed high-resolution genomic and expression analyses to compare the genomic content and expression correlates of 12q13-q14 amplification events in RMS with the corresponding findings in GBM, LUAD, and LPS. Our statistical approach identified "high-confidence" amplicons in the 12q13-q14 region along with genes that are significantly overexpressed in amplicon-positive samples. In comparison with amplification studies that identify a minimal common amplified region, the current statistical approach is less influenced by outliers and generally identifies a larger region that is amplified in many, but not all, cases. It should be noted that the endpoints of the high-confidence amplicon and the overexpressed genes can be affected by the selected fold-change or *P* value cutoffs; this issue may be at least partly responsible for situations in which the high-confidence amplified region does not fully correspond to the set of high-confidence overexpressed genes. In our previous study of the 12q13-q14 amplicon in FP RMS, a lower resolution Affymetrix GeneChip 250K array data set was used to define a 0.55 Mb minimal common amplified region that contained 27 genes, including CDK4 (11); this minimal common region closely overlaps our current 0.8 Mb high-confidence amplified region. These concordant results for the 12q13-q14 amplicon in FP RMS in 2 independent studies indicate that the smaller number of RMS cases compared with other tumor categories studied and differences in microarrays utilized did not adversely affect our copy number results.

Overexpressed oncogenes are critical factors that confer growth advantage to tumor cells harboring focal DNA amplifications. Our data indicate that CDK4, which encodes a cyclin-dependent kinase that promotes cell-cycle progression, is consistently amplified and overexpressed across multiple tumor types with 12q13-q14 amplification. In studies of amplification of the 17q21 genomic region in breast carcinoma and other tumor types, the ERBB2 oncogene has similarly been shown to play a central role (27–31). However, in addition to ERBB2, the consistent coamplification and overexpression of additional genes from the 17q21 region has prompted investigation of other potential oncogenes in this region, such as GRB7, that have functional significance when overexpressed and may provide additional selective pressure on the amplification process (32–36). We propose that coamplified genes may also be relevant as additional drivers in 12q13-q14 amplification and that such coamplified genes may vary among different tumor types. In the current study, we present SHMT2 as an example of such a critical coamplified driver that is recurrently amplified in FP RMS, but not in the other 3 tumor types. However, we acknowledge that there may be additional oncogenic drivers in the 12q13-q14 amplicon in FP RMS. In the available FP RMS cell line with the 12q13-q14 amplicon, SHMT2 was the only gene in the FP RMS–specific amplified region that exhibited differential expression relative to the amplicon-negative cell lines.

Although our approach establishes high-confidence amplified regions within the GBM, LUAD, or LPS categories, there may be cases in these categories with amplicons that extend beyond this high-confidence region to include SHMT2. The recent identification of SHMT2 amplification in some lung cancer cases (37) illustrates such a possibility. As described above, these SHMT2-containing amplicons also exist in The Cancer Genome Atlas (TCGA) lung cancer data set used in our analysis, but were not sufficiently common to be included in the high-confidence amplified region. Finally, it should be noted that SHMT2 amplification has recently been reported in lymphoma (22) and overexpression has been reported in several other cancer types (21, 23, 24), but the relationship to DNA copy number changes has not been determined.

One-carbon metabolism is essential for cell proliferation, as it functions to supply precursors for multiple cellular processes, including nucleotide synthesis, methylation, and reductive metabolism (18, 38). In this process, SHMT2 together with SHMT1 plays a critical role in generating 1-carbon units from glycine and serine. Depletion of these enzymes would be expected to lead to a detrimental outcome on cell growth. Indeed, growth suppression by SHMT2 knockdown has been shown in several cellular contexts (21, 23, 24). Our study demonstrates that SHMT2 inhibition results in such an effect in FP RMS cells. Although SHMT1 and SHMT2 exert similar functional activity, SHMT2 appears to play a more dominant role in regulating cell growth, as shown in several studies in which knockdown of SHMT2, but not SHMT1, significantly inhibits cell growth and oncogenic transformation (21, 23, 24). In accordance with this premise, we show in this study that growth suppression resulting from SHMT2 depletion cannot be rescued by overexpression of SHMT1 in Rh30 cells. Furthermore, we identified a substantial subset of FP RMS tumors that contain

a 12q13-q14 amplicon including the SHMT2 gene. The resulting increased SHMT2 expression in these FP RMS tumors leads to increased output of 1-carbon units and is hypothesized to confer growth advantage to these tumor cells. Our finding that amplicon-negative FP RMS cells with engineered expression of SHMT2 gain a growth advantage both in vitro and in vivo provides further evidence to support this hypothesis. We therefore propose that SHMT2 is an oncogenic driver in these amplicon-positive RMS tumors and is a potential target for cancer treatment.

Our findings show an inverse relationship between SHMT2 expression and sensitivity to SHIN1. This resistance may be explained by the mechanism by which SHIN1 exerts its inhibitory effect. SHIN1 binds SHMT1 and SHMT2 through a single direct enantiomer-enzyme interaction and results in an enantioselective enzyme inhibition (21). Therefore, higher SHMT2 levels require more SHIN1 molecules to adequately occupy and efficiently suppress the target protein. We speculate that patients with tumors expressing high SHMT2 levels are likely to be relatively resistant to direct inhibitors such as SHIN1 and require high doses, which may give rise to more side effects due to suppression of SHMT activity in normal cells. This inverse relationship of protein expression and sensitivity to a direct inhibitor of this protein has been previously described in RMS cells with CDK4 amplification (16), breast cancer cells with CDK6 amplification (39), and leukemia cells with BCR-ABL amplification (40, 41). Although our data show that low SHMT2-expressing FP RMS cell lines are more sensitive to SHIN1, it remains to be studied whether patients with low SHMT2-expressing tumors would benefit from treatment with a direct SHMT2 inhibitor such as SHIN1.

Based on our finding of relative resistance to direct SHMT2 inhibitors in high SHMT2-expressing RMS tumors, we explored indirect approaches to targeting the SHMT2 pathway. In particular, the 1-carbon units generated by SHMT2 are utilized in the downstream folate cycle, which can be suppressed by a number of inhibitors (42). In contrast to the ineffectiveness of SHIN1 in directly targeting high SHMT2-expressing cells, the folate inhibitor PEM is able to effectively treat FP RMS cells with high SHMT2 levels. This result suggests that signals downstream of SHMT2 can be rate limiting and thus 12q13-q14–amplified FP RMS cases may be particularly susceptible to drugs, such as folate inhibitors, that target these downstream steps. Based on previous findings that cancer cells adapt their downstream metabolic processes to increased SHMT2 expression to support rapid proliferation (43), we speculate that FP RMS cells develop "addiction" to high SHMT2 expression levels, rendering them more susceptible to the folate inhibitor. Targeting the folate cycle has been used for treatment of various cancers, and complete response has been documented in some subsets of patients (44); however, the tumor characteristics underlying this response to folate inhibitors remain unknown. A single clinical study included 8 RMS patients and reported no beneficial effects of PEM (45). However, given that 20%–30% of RMS tumors are FP and that 25% of FP tumors have 12q13-q14 amplification (11), it is likely that none of the recruited patients had a FP RMS tumor with SHMT2 amplification. We propose that SHMT2 amplification and overexpression constitute one molecular marker of increased susceptibility to these drugs. Moreover, clinical application of folate inhibitors is often limited by side effects (42, 46) resulting from the inhibition of the folate cycle in normal proliferating cells. As shown in our studies of FP RMS and NSCLC cell lines, we predict that higher responsiveness of FP RMS tumors containing the 12q13-q14 amplicon to the folate inhibitor will allow for lower doses of these drugs to be used, thus decreasing side effects and enabling patients to better tolerate chemotherapy.

Methods

Copy number analysis. For copy number analysis, FP RMS samples were previously genotyped on Illumina Omni 2.5M arrays (10); GBM, LUAD, and LPS were previously genotyped on the Affymetrix SNP Array 6.0; and raw probe-level data from TCGA were retrieved from the Genomic Data Commons (GDC) legacy archive (https://portal.gdc.cancer.gov/legacy-archive/search/f). Samples with both copy number and RNA-Seq data were chosen for subsequent analyses. Regions with copy number changes were identified using Nexus Biodiscovery 8.0 software, and data were GC corrected and segmented using the SNP-FASST2 algorithm, as previously described (10). Data were compared against the human reference genome NCBI Build 37, and copy number changes were plotted using probe level log relative ratios. High-gain and low-gain thresholds were set to 0.7 and 0.4, respectively. A sample was considered amplicon positive if copy number calls in the 12q13-q14 region passed the high-gain threshold (Table 1). Samples that contained copy number calls between 0.1 and 0.4 in these regions were inconclusive and therefore omitted from subsequent analyses. Additionally, samples that had copy number gain in 50% or more of the chromosomal arm, which by definition is not a focal amplification event, were included in the whole-chromosome gain category. The remaining samples, which had no copy number gains in the regions of interest, were classified as amplicon negative. Copy number changes were quantitatively examined by extracting probe median values, which corresponded to the median value of the probes in the segment. The data were interrogated to require at least 1.4-fold change in probe-median ratio relative to nonamplified cases.

Gene-expression analysis. RNA-Seq was previously performed on the Illumina HiSeq2000 system, and the corresponding RNA-Seq data were obtained from the GDC for all tumor types except RMS, which was obtained from the OncoGenomics database (https://pob.abcc.ncifcrf.gov/cgibin/JK). The data derived from RMS tumors were previously analyzed using the TopHat pipeline, and fragments per kilobase of transcript per million mapped reads (FPKM) values, which were $\log_2$ transformed, were used for downstream differential gene analysis. RNA-Seq data derived from the remaining tumor types were previously analyzed using the SeqWare pipeline, where gene expression estimates were obtained using the RNA-Seq by expectation maximization (RSEM) algorithm (47, 48). RSEM-normalized data were further $\log_2$ transformed for our downstream gene-expression analysis. Genes in the 12q13-q14 region were analyzed for differential gene expression between amplicon-positive and amplicon-negative samples with a 2.0 fold change cutoff.

PDX tumors. Thirteen PDX tumors were obtained from St. Jude Children's Research Hospital (Memphis, Tennessee, USA), Champions Oncology, Jackson Laboratory, Peter Houghton (UT Health San Antonio, San Antonio, Texas, USA), and Christine Heske (National Cancer Institute, Bethesda, Maryland, USA).

Table 2. Primers and shRNA target sequences

Gene	Primer sequences for qPCR of genomic DNA
D12Z3	Forward: AGTAAGTTCTTTGTGTTGCCTC
	Reverse: ACTGTTTCAAAACTGCTCTC
SHMT2	Forward: TGGATGAAATTGAGCTGCTG
	Reverse: AGCCCATCCATACTCACTGG
CDK4	Forward: GATCACGGGCCTTGTACACT
	Reverse: TTGTTGCTGCAGGCTCATAC
	Primer sequences for qRT-PCR
NEMP1	Forward: TGATTAGCAGAGAGGCCACA
	Reverse: AGTCACCCAGGTGGAGAATG
NAB2	Forward: AGTAGGAAAGGAGGTTGGCG
	Reverse: GACCCTGCAGCCCAGAC
SHMT2	Forward: TTGCTTCCCCAGTCTGAGTC
	Reverse: ACTTCTCTTTGTTTTGGGCG
R3HDM2	Forward: CTGTCTGTGCTGCTCTGGC
	Reverse: GGACCGAGATGATAACCAGG
GAPDH	Forward: ACATCAAGAAGGTGGTGAAGCAG
	Reverse: CAAAGGTGGAGGAGTGGGTGTC
	shRNA target sequences
sh1	CCGGAGAGTTGTGGACTTTAT
sh2	ACAAGTACTCGGAGGGTTATC
	Primers for cloning SHMT2 ORF
	Forward: ATGCAGATCTACGATGCTGTACTTCTCTTTGTTTTGG
	Reverse: TCATCTCGAGTCAATGCTCATCAAAACCAGG

Survival analysis. A published data set of RMS outcome and expression microarray data (17) was downloaded from ArrayExpress (E-TABM-1202). The expression array data were normalized and $\log_2$ transformed with GCRMA methods (R package: gcrma). Probe set 214095_at was used to quantify SHMT2 mRNA expression in the PAX3-FOXO1–positive RMS tumors in the data set. SHMT2 expression levels were categorized as low and high when expression was below and above the median, respectively. Association between SHMT2 expression and overall survival in patients with PAX3-FOXO1–positive RMS was analyzed using the survival package in R* (49).

Cell culture, constructs, and viral transduction. The sources of RMS cell lines and culture conditions were previously described (16). The RMS052 cell line was established from the PDX tumor (POBRMS052) provided by Christine Heske. Lung cancer cell lines were obtained from the DTP/DCTD Tumor Repository of the National Cancer Institute (Frederick, Maryland, USA). For growth assays, dialyzed FBS (MilliporeSigma, F0392) was used. All cell lines were verified by STR profiling and were tested every 3 months and confirmed negative for mycoplasma infection.

All control (SHC002) and SHMT2 (TRCN0000034804 and TRCN0000234656) lentiviral shRNA constructs were obtained from MilliporeSigma; target sequences are provided in Table 2. For ectopic expression of SHMT2, the open reading frame was amplified from Rh30 cDNA using the primers described in Table 2, cloned into a retroviral pMSCV expression vector, and verified by sequencing. Production of amphitropic retroviruses and lentiviruses and viral transduction were performed as previously described (50, 51).

Measurement of cellular NADPH. Cells were seeded in full-growth medium overnight and refreshed with assay medium for 48 hours before being harvested for NADPH measurement using the NADP/NADPH Quantification Kit (MAK038, MilliporeSigma). Cells were detached from culture dishes in cold PBS using a cell scraper, pelleted by centrifugation at 500*g* for 5 minutes, and lysed in NADPH/NAD lysis buffer. Lysates were deproteinized by filtering through 10 kDa cutoff Centricon filters (Amicon Ultra-0.5). NADPH levels were measured at 450 nm absorbance according to the manufacturer's instructions. The protein concentration of the unfiltered lysate was used for normalization.

Cell growth and tumorigenesis assays. Real-time growth was measured on the IncuCyte S3 system (Essen BioScience), which quantifies cell confluence over a period up to 96 hours in culture. Briefly, 1000 cells were plated per well in 100 μl complete growth medium in 96-well, clear-bottom plates. After 24 hours, growth medium was refreshed or replaced with 200 μl medium containing inhibitor or DMSO (control). Assay plates were imaged in the IncuCyte S3 system, under phase contrast, 4× magnification with automatic recording every 6 hours. Data were analyzed using IncuCyte software, which quantifies cell confluence values (and standard errors for multiple well replicates) at each time point. All IncuCyte assays were performed with replicates of 3 to 6 wells.

For clonogenic assays, 360 to 500 cells were seeded in 6 cm dishes and growth medium was refreshed every 3 days. The dishes were fixed with methanol and stained with Giemsa solution (MilliporeSigma) after 3 weeks of culture. Assays were performed in triplicate. For focus formation assays, 500–1000 cells were cocultured with 2×10^5 NIH 3T3 fibroblasts in 6 cm dishes for 3 weeks (Rh30) or 4 to 5 weeks (Rh41 and Rh5) before being fixed with methanol and stained with Giemsa.

For tumor engraftment in mice, 10^6 cells were injected intramuscularly into the gastrocnemius muscle of 6-week-old female mice (NOD.SCID/NCr strain 560, Charles River/NCI Research Models and Services) and tumor monitoring was performed as previously described (52).

Detection of the 12q13-q14 amplicons in cell lines by qPCR. Genomic DNA from RMS cell lines was extracted using the DNeasy Extraction Kit (QIAGEN), and qPCR was performed using the PowerUp SYBR Green Master Mix (Thermo Fisher Scientific) on the Viia7 Real-Time PCR System (Applied BioSystems). Specific oligonucleotide primers (synthesized by Eurofins Scientific USA) for CDK4 and SHMT2 were selected to generate 150 to 200 bp products, and the chromosome 12-specific centromeric amplicon (D12Z3; ref. 53) was used as a reference nonamplified region (Table 2). CDK4 and SHMT2 relative copy number was calculated by the $2^{-\Delta\Delta Ct}$ method, and normalized for the value in RD cells, which is not amplified in the 12q13-q14 region (16).

RNA- and protein-expression assays. Total RNA was extracted using TRIzol (Invitrogen), and cDNA was synthesized from random hexamers with the iScript cDNA Synthesis Kit (Bio-Rad), following the manufacturers' instructions. qPCR was performed with oligonucleotide primers (synthesized by Eurofins Scientific USA; Table 2).

Western blotting and signal detection were performed as previously described (54). Membranes were incubated overnight with antibodies against SHMT1 (1:1000, catalog 80715, Cell Signaling Technology), SHMT2 (1:1000, catalog 12762, Cell Signaling Technology), NAB2 (1:200, catalog sc-23867, Santa Cruz Biotechnology Inc.), and GAPDH (1:200, catalog sc-47724, Santa Cruz Biotechnology Inc.). Quantification of protein band intensity was performed using ImageJ software (NIH).

IC_{50} measurements of SHIN1 and PEM. To measure drug sensitivity, 10^3 cells were seeded in clear-bottomed 96-well plates in 100 μl growth medium before being treated in assay medium with control (DMSO) or 2-fold serial dilutions of SHIN1 (AOB36697, AOBIOUS) or PEM (HY-10820, MedChemExpress). DMSO was adjusted to 0.064% as the final concentration in all wells. The assay was performed in 4-well replicates for each treatment. Cell growth was monitored by confluence using the IncuCyte system. Mean confluence values at 96 hours of culture were used to calculate IC_{50} using the Quest Graph IC_{50} Calculator as previously described (55).

Study approval. All animal studies were approved by the NCI-Bethesda Animal Care and Use Committee (Bethesda, Maryland, USA).

Statistics. Partek Genomics Suite, version 6.6, was used to perform nonparametric Mann-Whitney *U* tests to determine statistical differences of copy number and gene-expression changes between amplicon-positive and amplicon-negative samples. Correction for multiple testing was performed with Bonferroni's correction method (adjusted $P \leq 0.05$). For IncuCyte assays, to determine the significance of growth differences at multiple intervals between various cell culture growth conditions, multiple *t* tests (for 2 conditions) or ANOVA tests (> 2 conditions) with correction for multiple comparisons using the Šidák-Bonferroni method were performed in Prism 8. The *P* values pertain to the last 6 time points of the growth curve. In other assays, Student's *t* test (2 tailed and type 2) was used. Data are presented as the mean ± SD or SEM, as indicated. In all tests, $P \leq 0.05$ was considered statistically significant. For Kaplan-Meier survival estimates of the association between gene expression and overall survival, log-rank statistic testing was performed using the survival package in R*.

Author contributions

THN, PLV, GEH, WS, and FGB conceived the project. PLV, GEH, WS, and FGB developed bioinformatics approaches. JFS and JK provided array and sequencing data. PLV generated bioinformatics data. THN conducted experiments. SB and BC assisted with key experiments and provided key reagents. THN, PLV, and FGB analyzed the data and prepared the manuscript. GEH, SB, BC, JFS, JK, and WS reviewed the manuscript. The assignment of authorship order among the co–first authors was decided based on seniority.

Acknowledgments

We thank Gregory Ducker (University of Utah), Joshua D. Rabinowitz (Princeton University), Ralph DeBerardinis (University of Texas Southwestern Medical Center), and Christine Heske and Arnulfo Mendoza (National Cancer Institute) for helpful advice. This research was supported by the Intramural Research Program of the National Cancer Institute and the Joanna McAfee Childhood Cancer Foundation.

Address correspondence to: Frederic G. Barr, Laboratory of Pathology, Center for Cancer Research, National Cancer Institute, 10 Center Drive, Room 2S235D, Bethesda, Maryland 20892-1500, USA. Phone: 301.480.7176; Email: barrfg@mail.nih.gov.

PLV's present address is: George Washington University School of Medicine and Health Sciences, Washington DC, USA.

GEH's present address is: University of Michigan Medical School, Ann Arbor, Michigan, USA.

1. Vogelstein B, Kinzler KW, eds. *The Genetic Basis of Human Cancer*. McGraw Hill Professional; 2002.
2. Albertson DG, et al. Chromosome aberrations in solid tumors. *Nat Genet*. 2003;34(4):369–376.
3. Tlsty TD, et al. Differences in the rates of gene amplification in nontumorigenic and tumorigenic cell lines as measured by Luria-Delbrück fluctuation analysis. *Proc Natl Acad Sci U S A*. 1989;86(23):9441–9445.
4. Wright JA, et al. DNA amplification is rare in normal human cells. *Proc Natl Acad Sci U S A*. 1990;87(5):1791–1795.
5. Beroukhim R, et al. The landscape of somatic copy-number alteration across human cancers. *Nature*. 2010;463(7283):899–905.
6. Weischenfeldt J, et al. Pan-cancer analysis of somatic copy-number alterations implicates IRS4 and IGF2 in enhancer hijacking. *Nat Genet*. 2016;49(1):65–74.
7. Lopez CK, et al. Ontogenic changes in hematopoietic hierarchy determine pediatric specificity and disease phenotype in fusion oncogene-driven myeloid leukemia. *Cancer Discov*. 2019;9(12):1736–1753.
8. Slamon DJ, et al. Use of chemotherapy plus a monoclonal antibody against HER2 for metastatic breast cancer that overexpresses HER2. *N Engl J Med*. 2001;344(11):783–792.
9. Iqbal N, Iqbal N. Human epidermal growth factor receptor 2 (HER2) in cancers: overexpression and therapeutic implications. *Mol Biol Int*. 2014;2014:1–9.
10. Shern JF, et al. Comprehensive genomic analysis of rhabdomyosarcoma reveals a landscape of alterations affecting a common genetic axis in fusion-positive and fusion-negative tumors. *Cancer Discov*. 2014;4(2):216–231.
11. Barr FG, et al. Genomic and clinical analyses of 2p24 and 12q13-q14 amplification in alveolar rhabdomyosarcoma: a report from the Children's Oncology Group. *Genes Chromosomes Cancer*. 2009;48(8):661–672.
12. Bridge JA, et al. Genomic gains and losses are similar in genetic and histologic subsets of rhabdomyosarcoma, whereas amplification predominates in embryonal with anaplasia and alveolar subtypes. *Genes Chromosomes Cancer*. 2002;33(3):310–321.
13. Williamson D, et al. Fusion gene-negative alveolar rhabdomyosarcoma is clinically and molecularly indistinguishable from embryonal rhabdomyosarcoma. *J Clin Oncol*. 2010;28(13):2151–2158.
14. Knuutila S, et al. DNA copy number amplifications in human neoplasms: review of comparative genomic hybridization studies. *Am J Pathol*. 1998;152(5):1107–1123.
15. Myllykangas S, et al. Specificity, selection and significance of gene amplifications in cancer. *Semin Cancer Biol*. 2007;17(1):42–55.
16. Olanich ME, et al. CDK4 amplification reduces sensitivity to CDK4/6 inhibition in fusion-positive rhabdomyosarcoma. *Clin. Cancer Res*. 2015;21(21):4947–4959.
17. Missiaglia E, et al. PAX3/FOXO1 fusion gene status is the key prognostic molecular marker in rhabdomyosarcoma and significantly improves current risk stratification. *J Clin Oncol*. 2012;30(14):1670–1677.
18. Ducker GS, Rabinowitz JD. One-carbon metabolism in health and disease. *Cell Metab*. 2017;25(1):27–42.
19. Fan J, et al. Quantitative flux analysis reveals folate-dependent NADPH production. *Nature*. 2014;510(7504):298–302.
20. Anderson DD, Stover PJ. SHMT1 and SHMT2 are functionally redundant in nuclear de novo thymidylate biosynthesis. *PLoS One*. 2009;4(6):e5839.
21. Ducker GS, et al. Human SHMT inhibitors reveal defective glycine import as a targetable metabolic vulnerability of diffuse large B-cell lymphoma. *Proc Natl Acad Sci U S A*. 2017;114(43):11404–11409.
22. Parsa S, et al. The serine hydroxymethyltransferase-2 (SHMT2) initiates lymphoma development through epigenetic tumor suppressor silencing. *Nat Cancer*. 2020;1(6):653–664.
23. Woo CC, et al. Downregulating serine hydroxymethyltransferase 2 (SHMT2) suppresses tumorigenesis in human hepatocellular carcinoma. *Oncotarget*. 2016;7(33):53005–53017.
24. Wei Z, et al. Deacetylation of serine hydroxymethyl-transferase 2 by SIRT3 promotes colorectal carcinogenesis. *Nat Comms*.

2018;9(1):4468.
25. Moran DM, et al. KRAS mutation status is associated with enhanced dependency on folate metabolism pathways in non-small cell lung cancer cells. *Mol Cancer Ther*. 2014;13(6):1611–1624.
26. Weeks LD, et al. Uracil-DNA glycosylase expression determines human lung cancer cell sensitivity to pemetrexed. *Mol Cancer Ther*. 2013;12(10):2248–2260.
27. Moasser MM. The oncogene HER2: its signaling and transforming functions and its role in human cancer pathogenesis. *Oncogene*. 2007;26(45):6469–6487.
28. Hynes N. The biology of erbB-2/nue/HER-2 and its role in cancer. *Biochim Biophys Acta*. 1994;1198(2-3):165–184.
29. Slamon DJ, et al. Human breast cancer: correlation of relapse and survival with amplification of the HER-2/neu oncogene. *Science*. 1987;235(4785):177–182.
30. Reichelt U, et al. Frequent homogeneous HER-2 amplification in primary and metastatic adenocarcinoma of the esophagus. *Mod Pathol*. 2006;20(1):120–129.
31. Baselga J, Swain SM. Novel anticancer targets: revisiting ERBB2 and discovering ERBB3. *Nat Rev Cancer*. 2009;9(7):463–475.
32. Haverty PM, et al. High-resolution genomic and expression analyses of copy number alterations in breast tumors. *Genes Chromosomes Cancer*. 2008;47(6):530–542.
33. Kao J, Pollack JR. RNA interference-based functional dissection of the 17q12 amplicon in breast cancer reveals contribution of coamplified genes. *Genes Chromosomes Cancer*. 2006;45(8):761–769.
34. Stein D, et al. The SH2 domain protein GRB-7 is co-amplified, overexpressed and in a tight complex with HER2 in breast cancer. *EMBO J*. 1994;13(6):1331–1340.
35. Bièche I, et al. Two distinct amplified regions at 17q11-q21 involved in human primary breast cancer. *Cancer Res*. 1996;56(17):3886–3890.
36. Zhu Y, et al. Amplification and overexpression of peroxisome proliferatoractivated receptor binding protein (PBP/PPARBP) gene in breast cancer. *Proc Natl Acad Sci U S A*. 1999;96(19):10848–10853.
37. Lee GY, et al. Comparative oncogenomics identifies PSMB4 and SHMT2 as potential cancer driver genes. *Cancer Res*. 2014;74(11):3114–3126.
38. Newman AC, Maddocks ODK. One-carbon metabolism in cancer. *Br J Cancer*. 2017;116(12):1499–1504.
39. Yang C, et al. Acquired CDK6 amplification promotes breast cancer resistance to CDK4/6 inhibitors and loss of ER signaling and dependence. *Oncogene*. 2017;36(16):2255–2264.
40. Gadzicki D, et al. BCR-ABL gene amplification and overexpression in a patient with chronic myeloid leukemia treated with imatinib. *Cancer Genet Cytogenet*. 2005;159(2):164–167.
41. Milojkovic D, Apperley J. Mechanisms of resistance to imatinib and second-generation tyrosine inhibitors in chronic myeloid leukemia. *Clin Cancer Res*. 2009;15(24):7519–7527.
42. Visentin M, et al. The antifolates. *Hematol Oncol Clin North Am*. 2012;26(3):629–648.
43. Kim D, et al. SHMT2 drives glioma cell survival in ischaemia but imposes a dependence on glycine clearance. *Nature*. 2015;520(7547):363–367.
44. Jackman AL, et al. Targeting thymidylate synthase by antifolate drugs for the treatment of cancer. In: Stephen Neidle, ed. *Cancer Drug Design and Discovery*. Academic Press; 2008:198–226
45. Warwick AB, et al. Phase 2 trial of pemetrexed in children and adolescents with refractory solid tumors: a Children's Oncology Group study. *Pediatr Blood Cancer*. 2012;60(2):237–241.
46. Pierard-Franchimont C, et al. Toxic epidermal necrolysis and antifolate drugs in cancer chemotherapy. *Curr Drug Saf*. 2012;7(5):357–360.
47. O'Connor BD, et al. SeqWare Query Engine: storing and searching sequence data in the cloud. *BMC Bioinformatics*. 2010;11(Suppl 12):S2.
48. Li B, Dewey CN. RSEM: accurate transcript quantification from RNA-Seq data with or without a reference genome. *BMC Bioinformatics*. 2011;12(1):323–316.
49. Therneau T. *Modeling Survival Data: Extending the Cox Model*. Springer; 2000.
50. Brummelkamp TR. A system for stable expression of short interfering RNAs in mammalian cells. *Science*. 2002;296(5567):550–553.
51. Meerbrey KL, et al. The pINDUCER lentiviral toolkit for inducible RNA interference in vitro and in vivo. *Proc Natl Acad Sci U S A*. 2011;108(9):3665–3670.
52. Pandey PR, et al. PAX3-FOXO1 is essential for tumour initiation and maintenance but not recurrence in a human myoblast model of rhabdomyosarcoma. *J Pathol*. 2017;241(5):626–637.
53. Vermeesch JR, et al. A physical map of the chromosome 12 centromere. *Cytogenet Genome Res*. 2003;103(1–2):63–73.
54. Nguyen HT, et al. Viral small T oncoproteins transform cells by alleviating hippo-pathway-mediated inhibition of the YAP proto-oncogene. *Cell Rep*. 2014;8(3):707–713.
55. Sebaugh JL. Guidelines for accurate EC50/IC_{50} estimation. *Pharmaceut Statist*. 2011;10(2):128–134.